# Liquid and Glass Polymorphism in a Monatomic System with Isotropic, Smooth Pair Interactions

Joel Y. Abraham,[†] Sergey V. Buldyrev,[‡] and Nicolas Giovambattista*,[†]

[†]Department of Physics, Brooklyn College of the City University of New York, Brooklyn, New York 11210, United States
[‡]Department of Physics, Yeshiva University, New York, New York 10033, United States

**ABSTRACT:** Systems of particles with interactions given by the Jagla core-softened pair potential are known to exhibit water-like thermodynamic anomalies and a liquid—liquid phase transition. The drawback of the Jagla potential is that it is characterized by discontinuous forces acting between particles and thus is not suitable for standard molecular dynamics (MD) simulations. Here we introduce a smooth version of the Jagla potential based on two Fermi distributions and study the properties of a system of particles interacting via this new "Fermi—Jagla" pair potential by using standard MD simula-



tions. We find that the liquid based on the Fermi—Jagla potential retains most of the properties of the liquid based on the original Jagla potential. Namely, it exhibits the following water-like anomalies: (i) decrease of density, (ii) increase of compressibility, $\kappa_T(T,P)$, and (iii) increase of isobaric specific heat, $C_P(T,P)$, upon isobaric cooling, and (iv) increase of diffusivity upon isothermal compression. The Fermi—Jagla potential also exhibits (i′) density minima, (ii′) compressibility minima, (iii′) isobaric specific heat minima upon isobaric cooling, and (iv′) diffusivity minima upon isothermal compression. As in the Jagla model case, we find a liquid—liquid phase transition (LLPT) and a liquid—liquid critical point in the equilibrium liquid. Contrary to the case of the original Jagla model liquid, the LLPT line for the Fermi—Jagla potential has a negative slope in the P—T plane that extends well above the crystallization temperature. This feature makes the Fermi—Jagla potential a better candidate to reproduce the behavior of tetrahedral liquids including water, for which the LLPT line observed in simulations has also negative slope. In the glass state, the Fermi—Jagla pair potential results in reversible polyamorphism between low- and high-density amorphous solids (LDA and HDA, respectively). We also find that HDA results from pressure-induced amorphization of the model's low pressure crystal, as observed in water and other materials. The Fermi—Jagla pair potential, being a smooth function of the interparticle separation, can be easily implemented in standard MD simulation codes. Moreover, since spontaneous crystallization for the Fermi—Jagla potential can be avoided by fast cooling, it can be used to study the phenomenology of glasses.
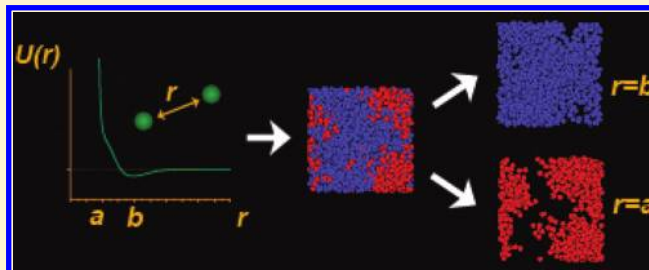
## I. INTRODUCTION

Most substances have one liquid phase and can be brought into one glass state, e.g., by rapidly cooling the liquid. However, roughly 25 years ago, experiments at low temperature showed that a single substance, water, could exist in at least two different glass states; such glass states being separated by an apparent first-order phase transition.[1,2] The observation of more than one glass state in a single substance gave origin to the concept of "poly-amorphism" (see, e.g., refs 3—7). Polyamorphism is not limited to the glass state (glass polymorphism) but can also occur in the liquid state (liquid polymorphism). Although more than 40 years ago theoreticians noticed that liquid polymorphism could exist in classical liquids (see, e.g., refs 8 and 9), such an idea was not set on firm grounds until the work of Poole et al.[10] based on computer simulations of water. These simulations indicate that water could have, in addition to two glass states, two different liquid states. Their simulations showed that these two liquid states, low- and high-density liquid (LDL and HDL, respectively), were separated by a first-order phase transition line ending in a liquid—liquid critical point (LLCP).

At present, there is a large number of substances that are known to exhibit liquid or glass polymorphism. Examples include monatomic systems, such as silicon,[11] germanium,[12] and phosphorus,[13,14] molecular systems, such as water,[1,2] as well as multicomponent systems, such as $SiO_2$,[15] $Ce_{75}Al_{25}$ metallic glasses,[16,17] and $Al_2O_3—Y_2O_3$ melts.[18] Experimental evidence indicating the existence of an LLPT in the molecular systems *n*-butanol,[19,20] triphenyl phosphite (TPP),[21−23] and binary mixtures containing TPP[24] have also been reported. Liquid polymorphism may not be a rare phenomenon and many substances have been suggested to exhibit LLPT (see, e.g., refs 25—27). Many of these polyamorphic substances are relevant to technological applications. For example, the garnet $Y_3Al_5O_{12}$ in the $Al_2O_3—Y_2O_3$ system is commonly used as a host material in
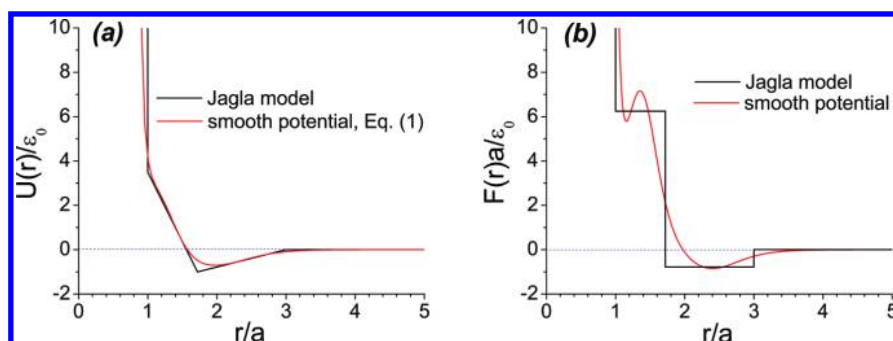
**Figure 1.** (a) Comparison of the Fermi—Jagla pair interaction potential studied in this work (red curve) and the Jagla pair potential (black curve) previously proposed to model the properties of water. (b) The Jagla model results in an interparticle force that is a discontinuous function of the particle separation, $r$ (black curve). The Fermi—Jagla potential is smooth, with a pair interaction force that is a continuous function of $r$ (red curve).

various solid-state lasers[28] and silicon plays a central role in electronic and photovoltaic applications. Water, an ubiquitous liquid in Earth, is also relevant in technological application and, in particular, it plays a central role in biology and chemistry.[29,30] The presence of liquid—liquid or glass—glass transitions in these substances, and possibly the existence of an LLCP, can be crucial in the determination of the thermodynamic, structural, and dynamical properties of these substances. In particular, the presence of an LLCP could affect the properties of these substance at temperatures and pressures in the phase diagram far from the location of the LLCP, originating anomalous properties in these liquids. It follows that the performance of these substances in engineering applications, and their effect in biological systems for the case of water, could be largely affected by the presence of more than one liquid states.

The field of polyamorphism is relatively new and much effort has been spent in order to obtain a general picture of the thermodynamic and dynamical properties of polyamorphic substances. Much of our knowledge of polyamorphic substances is based on computer simulations. This is, in part, because polyamorphism in experiments may occur at low-temperatures where crystallization cannot be avoided, such as in the case of liquid water, or at thermodynamic conditions where experiments may be difficult to perform, e.g., high pressures.[31] Fortunately, model systems for computer simulations are available where these problems can be avoided. Examples include realistic computer simulation models of water,[32−35] silica,[36] silicon,[37−39] and germanium.[12,40] In addition, there is a large family of monatomic model systems that can also exhibit polyamorphism. In these model systems, particles interact via isotropic pair interaction potentials that are characterized by a hard-core decorated by a core-softened part;[41,42] an example of such potentials is shown in Figure 1a. Core-softened pair potentials have been proposed as models for metals, such as cerium and cesium,[41,42] polymer solutions,[43] as well as coarse-grain models of molecular systems, such as water.[44] With appropriate parametrization, core-softened potentials are remarkable model liquids that exhibit anomalous properties observed, e.g., in tetrahedral liquids such as silica and water.[45] They can also exhibit polyamorphism, both in the liquid[46−49] and glass state.[45,50,51] A particular subfamily of core-softened pair potentials, the "ramp" and Jagla models, have been studied extensively in the past due to the similarities in their phase diagram with that of water (see, e.g., the review articles 52 and 53). In some cases, such similarities are not only qualitative but can be extended to the quantitative level.[44]

In this work we introduce a core-softened, isotropic, pair interaction potential based on the Jagla model[47,48] [see Figure 1a] in which the linear ramps are replaced by two Fermi functions. Contrary to the Jagla pair potential case, this new Fermi—Jagla pair potential is smooth, resulting in forces between particles that are continuous functions of the interparticle separations (see Figure 1b). Although slight modifications in pair interaction potentials can result in drastic changes in the corresponding liquid's properties, we find that the Fermi—Jagla potential preserves the main properties of the original Jagla model. Specifically, it exhibits both liquid and glass polymorphism and a LLCP in the equilibrium liquid domain, well separated from the crystallization region. The Fermi—Jagla potential has an advantage, with respect to the Jagla potential, that it shows a liquid—liquid phase transition (LLPT) line with a negative slope in the $P$ vs $T$ plane. Identifying monatomic model systems with a negatively sloped LLPT line has been challenging,[54] while it is an important feature of the majority of real polyamorphic systems, such as silicon,[55] yttrium oxide—aluminum oxide melts,[56] and water,[6] in which the LLPT line in the $P$ vs $T$ plane has, or it is expected to have, a negative slope.

This work is organized as follows. In the next section, we define the Fermi—Jagla pair interaction potential used in this work and discuss the computer simulation details. In section III we discuss the phase diagram of the model, including the LLPT and the water-like anomalous properties that the Fermi—Jagla liquid exhibits at temperatures above the LLCP. Both thermodynamic and dynamical properties are described. In section IV, we show that the Fermi—Jagla system exhibits glass polymorphism. In particular, it is shown that MD simulations using the Fermi—Jagla potential can indeed reproduce the transformation between low- and high-density amorphous solids (LDA and HDA, respectively) upon compression and decompression, which are observed in polymorphic glasses. We also observe the pressure-induced amorphization of the model's low-pressure crystal, which results in HDA. A summary of the results is provided in section V.

## II. COMPUTER SIMULATIONS

**Fermi—Jagla Pair Interaction Potential.** We perform molecular dynamics (MD) simulations of a system of particles interacting via a smooth pair interaction potential defined in eq 1 and shown in Figure 1a. Our potential is based on the Jagla potential[47,48] in which linear ramps are replaced by Fermi distributions and the hard sphere repulsion is replaced by a power law repulsion.

**Table 1. Pair Interaction Potential Parameters Used in eq 1**[a]

| $n$ | $A_0$ | $A_1$ | $A_2$ | $B_0$ | $B_1$ | $B_2$ |
|-----|-------|-------|-------|-------|-------|-------|
| 20 | 4.56 | 28.88 | 1.36 | 1.00 | 3.57 | 2.36 |

[a] See Figure 1a.

The Jagla potential was originally proposed to model the behavior of water and silica[45] and has been extensively studied in the past.[46,51,54] A smooth version of the Jagla potential has been introduced by Jagla himself[45] to study polymorphic glasses of binary mixtures; the choice of using binary mixtures in ref.,[45] instead of monodisperse liquids, was justified in order to avoid crystallization. The functional form of our potential is simpler than the one proposed by Jagla. Also our potential is infinitely differentiable for any values of intermolecular distance, while the Jagla potential diverges at the hard-core distance. As the original Jagla potential, the Fermi—Jagla potential also has a hard-core part at short particle separations, $r$, a core-softened part at intermediate particle separations, followed by an attractive part at larger particle separations. This potential is characterized by two length scales, defined by the effective hard-core distance $a$, and the wide potential minimum located at $r \approx 2a$ (we note, however, that the effective length scales of this pair potential are $r \approx a$ and $r \approx 1.7a$; see section III.A).

The functional form of the Fermi—Jagla pair interaction potential of Figure 1(a) is given by

$$U(r) = \epsilon_0 \left[ (a/r)^n + \cfrac{A_0}{1 + \exp\left[\dfrac{A_1}{A_0}(r/a - A_2)\right]} \right.$$
$$\left. - \cfrac{B_0}{1 + \exp\left[\dfrac{B_1}{B_0}(r/a - B_2)\right]} \right] \tag{1}$$

The parameters $A_i$ and $B_i$ ($i = 0,1,2$) are provided in Table 1 (the parameters $\epsilon_0$ and $a$ are irrelevant since they define respectively the unit of energy and length). The advantage of the pair potential given in eq 1, relative to the Jagla potential, is that it is a smooth function of $r$, i.e., its first derivative with respect to $r$ is a continuous function. It follows that the forces between particles resulting from eq 1 are continuous functions of $r$, see Figure 1b.

Smooth isotropic potentials that exhibit water-like anomalies have been proposed in the past; see, e.g., refs 43, 49, and 57—62. The success of such potentials to exhibit water-like properties varies and, not surprisingly, the properties of the corresponding liquids are extremely sensitive to the details of the pair interaction potential considered (see, e.g., refs 48, 58, and 63—67). The goal of this work is to obtain a smooth pair interaction potential that exhibits not only the anomalous properties of liquid water but also polyamorphism in both the liquid and glassy state. The Jagla potential exhibits polyamorphism in the liquid and glassy state[45,46,50,51] and, hence, our choice of using it as a starting point to define $U(r)$.

The rationale behind the particular functional form of $U(r)$ in eq 1 is to generate a family of pair interaction potentials that can be easily tuned with the change of a few parameters. The three terms in eq 1 have a simple interpretation in defining the shape of $U(r)$. Specifically, the first term is mainly responsible of the hard-core part of the pair potential and prevents particles from overlapping with one another. The second term is a Fermi distribution (where $r$ plays the role of energy) that is mainly responsible for the core-softened part of $U(r)$. The parameters $A_0$ and $A_2$ define the amplitude and location (Fermi's energy) of this distribution, respectively. The slope of the Fermi distribution, at its Fermi energy, is controlled by the parameter $A_1$ and can be used to alter the slope of the core-softened part (i.e., the negatively sloped ramp) of $U(r)$. The third term of eq 1 is an inverted Fermi distribution and is mainly responsible for the positively sloped ramp of $U(r)$. The parameters $B_0$ and $B_2$ define the amplitude and location (Fermi energy) of the distribution, whereas $B_1$ can be used to tune the slope of $U(r)$ at $r \approx B_2$. In this work, we will consider the parameters given in Table 1. They have been chosen in order for the smooth pair interaction potential to reproduce the forces between particles defined in the Jagla model, at separations $r \approx 1.2$ and 2.2 [see Figure 1b]. These values of $r$ correspond approximately to the location of the midpoint of the ramps in the Jagla pair interaction potential [Figure 1a].

**Simulation Details.** All simulations are performed for a system of $N = 1728$ particles. Simulations in the liquid state are performed at constant volume and temperature (NVT-ensemble); constant pressure and temperature (NPT-ensemble) simulations are performed to study the glass state. The temperature is controlled by rescaling periodically the particle's velocities[68] every 100 simulation time steps. Quantities are reported in reduced units. Energies and temperatures are reported in units of $\epsilon_0$ and $\epsilon_0/k_B$, respectively, where $k_B$ is the Boltzmann constant. Distances are reported in units of $a$, which corresponds approximately to the hard-core distance of $U(r)$ [see Figure 1a]. Times are give in units of $a(m/\epsilon_0)^{1/2}$. This choice of units define the units of all other quantities; for example, pressure and density units are $\epsilon_0/a^3$ and $m/a^3$, respectively. NVT ensemble simulations are performed for at least $9.9 \times 10^6$ time steps, starting from an equilibrated, high-temperature liquid configuration. The particle's mean-square displacement obtained at a given $T$ indicates that particles diffuse for at least 2—3 particle diameters, suggesting that simulations are run for long enough times in order for equilibrium to be reached. The computer simulation time step is d$t = 0.001$; a cutoff distance of $r_c = 4.0$ is used in the calculation of the pair interactions.

We also perform cooling simulations in the NVT ensemble to obtain approximate isochores in the $P-T$ phase diagram of the system. In these cases, the temperature of the thermostat is reduced by $\Delta T = 10^{-5}$ every time interval $\Delta t = 0.1$, resulting in a fixed cooling rate of $q_T \equiv \Delta T/\Delta t = 10^{-4}$ ($q_T$ units are $\epsilon_0^{3/2}/(m^{1/2}k_B a)$).

Computer simulations of compression and decompression of glasses and crystals are performed at constant temperature and pressure (NPT ensemble). In these cases, the temperature of the system is kept constant while the pressure is controlled using a Berendsen barostat.[69] Upon compression or decompression, the barostat pressure is increased by $\Delta P = \pm 1.27 \times 10^{-7}$ every time step ($\Delta t = 0.001$), resulting in a compression/decompression rate of $q_P = \pm 1.27 \times 10^{-4}$ ($q_P$ units are $\epsilon_0^{3/2}/(m^{1/2}a^4)$).

A quantitative connection between units and rates from computer simulations using the Jagla model and physical units for the case of real water is provided in ref 51. The same connection between simulations and water physical units of ref 51 applies to this work. In particular, a separation between particles of $r = a$, in our model liquid, corresponds to the distance between nearest neighbors in water, $\sim$0.27 nm. Moreover, by

14231

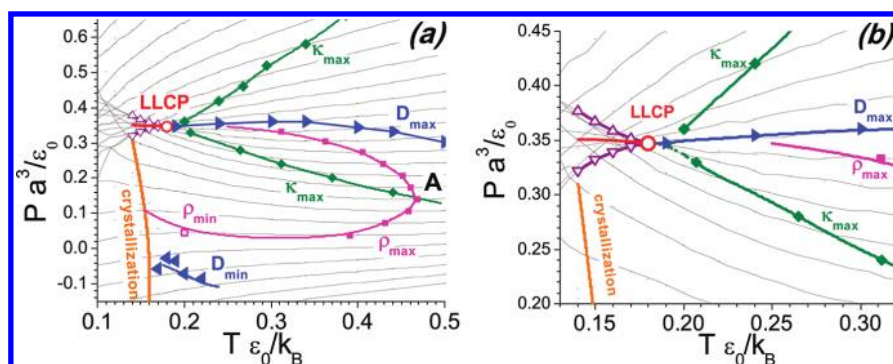dx.doi.org/10.1021/jp205098a |*J. Phys. Chem. B* 2011, 115, 14229—14239

**Figure 2.** (a) phase diagram of a system of particles interacting via the Fermi—Jagla pair potential [Figure 1a]. The system exhibits a liquid—liquid first-order phase transition line (red curve) that ends at a liquid—liquid critical point (LLCP, empty red circle). The LDL and HDL spinodal lines are represented by purple up- and down-triangles, respectively. A magnification of the LLCP region is shown in (b). The supercritical liquid exhibits extrema lines in dynamical and thermodynamical properties. Magenta line is the maximum (full squares, $\rho_{max}$) and minimum (empty square, $\rho_{min}$) density line. Green lines are maximum compressibility lines (full diamonds, $\kappa_{max}$). Blue lines are the maximum (right-triangles, $D_{max}$) and minimum (left-triangles, $D_{min}$) diffusivity lines. The low-pressure $\kappa_{max}$ and $\rho_{max}$ lines intersect one another at point "A", where the slope of the $\rho_{max}$ line is infinite. Crystallization occurs only at low pressures; the orange curve indicates approximately the temperature at which the liquid spontaneously crystallizes. Thin black lines are isochores obtained upon cooling the liquid continuously; black dots are results from constant volume and temperature simulations.

using the same argument of ref 44, one can associate a particle in our model liquid to one water molecule plus one-quarter of each of its four nearest neighbors (two molecules in total).

## III. LIQUID POLYMORPHISM: PHASE DIAGRAM AND ANOMALOUS PROPERTIES

Figures 2a and 2b show the phase diagram for a system of particles interacting via the Fermi—Jagla pair potential. Figure 2a is qualitatively similar to the phase diagram obtained in ref 70 from discrete MD simulations using the Jagla pair interaction potential. In particular, it exhibits an LLPT line ending in an LLCP. It also shows extrema lines in various thermodynamic properties, such as density and compressibility, implying that the liquid exhibits some of the anomalous properties found in water, such as the increase of compressibility upon isobaric cooling and the presence of density maxima. The properties of polyamorphic, monatomic liquids composed of particles interacting via core-softened isotropic pair potentials are discussed in detail in, e.g., refs 52 and 53. In this section, we describe briefly the features of the phase diagram of Figure 2 and compare it with the phase diagram of the Jagla model.

**A. Liquid—Liquid Phase Transition.** Figure 2a shows the liquid isochores in the $P-T$ plane corresponding to the potential of eq 1. The intersection of these isochores indicates that the system exhibits a LLPT. Figure 2b shows the region of the phase diagram where the LLPT occurs. The LLCP is located at $T_{C'} \approx 0.18$ and $P_{C'} \approx 0.35$. Figure 2b also shows the LDL and HDL spinodal lines at $T < T_{C'}$ which define the boundaries of the regions where these liquids can be found.

One of the most interesting observations of Figure 2(b) is that the slope of the LLPT line is slightly negative, $dP/dT|_{coexistence} = -0.08$ at $T \approx 0.17$. From the Clapeyron relation,[71] it follows that LDL has less entropy (i.e., is more ordered) than HDL. Experiments in common polyamorphic substances, such as water,[6] silicon,[55] and yttrium oxide-aluminum oxide melts,[56] indicate that, at least for these cases, the slope of the LLPT line should be negative. In this regard, we note that the Jagla model liquid, with the parametrization corresponding to Figure 1a, exhibits a LLPT line that is positively sloped in the $P-T$ plane. Although reparameterization of the Jagla model can lead to negatively
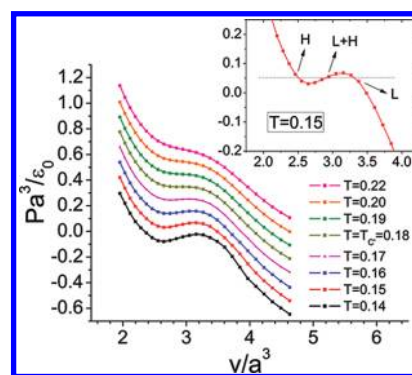


**Figure 3.** Liquid isotherms in the $P-v$ plane ($v = V/N$). Isotherms at $T = 0.14$, $0.15$, $0.16$, and $0.17$ are shifted respectively by $\Delta P = -0.4, -0.3, -0.2$, and $-0.1$; isotherms at $T = 0.19$, $0.20$, and $T = 0.22$ are shifted by $\Delta P = 0.1$, $0.2$, and $0.3$, respectively. Above the LLCP temperature, $T_{C'} = 0.18$, isotherms decrease monotonically with $v$ while, at $T < T_{C'}$, isotherms exhibit unphysical oscillations indicating phase separation into LDL and HDL. The isotherm at $T = 0.15$ is shown in the inset. The horizontal line indicates the coexistence pressure (shifted by $\Delta P = -0.3$) obtained by applying the "lever rule".[71] The radial distribution functions of the liquid at the state points indicated by L, H, and L + H [which correspond to pure LDL ($v = 3.375$), HDL ($v = 2.460$), and a mixture of LDL and HDL ($v = 2.945$), respectively] are shown in Figure 4.

sloped LLPT lines,[54] crystallization in these cases easily occurs and makes it difficult the access of the LDL-HDL coexistence region using computer simulations.[54] As shown in Figure 2a, this is not the case for the smooth pair interaction potential of eq 1 since the crystallization line is well-separated from the LLCP. As shown in Figure 2, crystallization occurs only in the LDL phase. At high pressure, crystallization of HDL is not observed in the present simulations, HDL forming a glass at very low temperatures. Similar observations, i.e., crystallization of LDL and absence of crystallization of HDL, were reported in ref 52 from MD simulations using the Jagla model. It is probable that the fast crystallization of LDL in both the Jagla and Fermi—Jagla models is due to the similarities in the structure of LDL and HCP crystal [see Figures 4a and 9c].

The LLCP, LL coexistence, and spinodal lines in Figure 2 are determined from Figure 3, which shows the $P(v)$ isotherms of
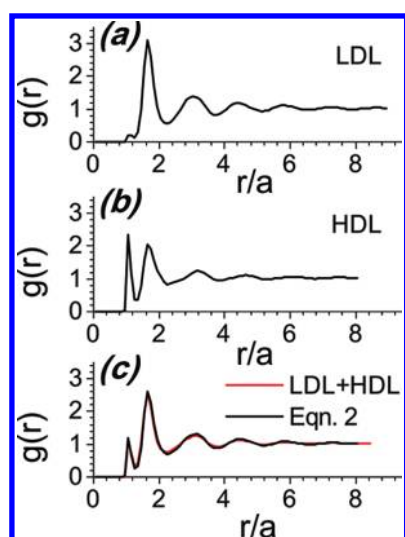
14232

dx.doi.org/10.1021/jp205098a |*J. Phys. Chem. B* 2011, 115, 14229–14239

**Figure 4.** Radial distribution functions (RDFs) of (a) LDL, (b) HDL, and (c) a mixture of LDL and HDL at $T = 0.15$. The volume of the liquids are indicated in the inset of Figure 3 by the symbols $L$, $H$, and $L + H$, respectively. Shown in (c) are the RDFs of the mixture and the corresponding approximation given by eq 2, using the RDFs of LDL and HDL shown in (a) and (b). The RDFs in (c) practically overlap, as expected if the liquid is indeed experiencing an LDL-HDL first-order phase transition at $T = 0.15$.

the liquid at different temperatures; $v = V/N$. The $P(v)$ isotherms show an unphysical region of negative compressibility for $T < 0.18$, indicating that the system separates into two liquid phases, LDL and HDL, at these temperatures. The nonmonotonic behavior of $P(v)$ is analogous to the van der Waals loops in the isotherms of real gases. In the MD simulations the nonmonotonic behavior of $P(v)$ is observed due to periodic boundary conditions allowing the two coexisting phases to form a fluctuating boundary connecting the opposite sides of the simulation box. The surface tension of this boundary creates a negative contribution to the pressure which becomes stronger as the volume decreases. At $T = T_{C'} = 0.18$, $P(v)$ shows an inflection point at $P = P_{C'} \approx 0.35$ and $v = v_{C'} \approx 2.9$ (corresponding to a density number $N/V \approx 0.345$), which defines the location of the LLCP. The maxima and minima of the $P(v)$ isotherms define the LDL and HDL spinodal lines, respectively, whereas the coexistence line in Figure 2 is obtained by applying the "lever rule" to the $P(v)$ isotherms.[71] At $T = 0.15$, the volume per particle of HDL and LDL at the coexisting pressure are $v_{HDL} = 2.502$ and $v_{LDL} = 3.322$ (see inset of Figure 3), resulting in a molar volume ratio of $v_{HDL}/v_{LDL} \approx 0.75$. Interestingly, the molar volume ratio of water HDA and LDA at $T = 130-140$ K is $v_{HDA}/v_{LDA} = 0.79$; see Figure 2 of ref 72. We note that the lowest temperature at which we can determine reliable isotherms is $T = 0.14$.

The structural properties of LDL and HDL are similar to those observed in the case of the Jagla model liquid. The radial distribution functions (RDFs) of LDL and HDL at $T = 0.15$ are shown in Figures 4a and 4b, respectively. These RDFs correspond to the state points denoted as "L" and "H" in the inset of Figure 3. In LDL, nearest neighbors are separated in average by a distance $r_2 = 1.7$, as indicated by the location of the first peak of the RDF shown in Figure 4a. This distance is slightly smaller than the location of the minimum in the Fermi−Jagla pair potential shown in Figure 1a. As LDL transforms to HDL, nearest neighbors move closer to each other, from an average

separation $r_2$ to a typical distance $r_1 = 1$. These characteristic distances are defined by the location of the first two peaks in the RDF shown in Figure 4c. The value $r_1$ corresponds approximately to the hard-core radius of the smooth pair interaction potential shown in Figure 1a. We note that the ratio $r_1/r_2 \approx 0.59$ is close to the ratio between the first and second shell radii in water, $\sim 0.6$. The relevance of the value for $r_1/r_2$ in order for a monatomic liquid to reproduce water-like properties has been discussed in detail in refs 66 and 67 based on computer simulations of Jagla model liquids with no attractive part (these liquids do not exhibit LLPTs).

It is expected that if there is a phase transition between LDL and HDL, the RDF of the liquid in the coexistence region should be well-approximated by a linear superposition of the RDFs of LDL and HDL. To show that this is the case for the present system, we calculate the RDF of the system at the state point indicated as "L+H" in the inset of Figure 3. The RDF for the mixture is shown in Figure 4c. We also include the RDF resulting from the approximation

$$g(r) = x \, g_{LDL}(r) \, + \, (1 - x) \, g_{HDL}(r) \qquad (2)$$

where $x = 0.46$ and $(1 - x)$ are the fractions of the system in the LDL and HDL phase, respectively, and are obtained from the inset of Figure 3a using the "lever rule".[71] Figure 4c shows that indeed the RDF of the mixture is well-approximated by eq 2.

**B. Liquid Anomalous Properties in the Supercritical Region.** The existence of the LLCP in Figure 2a implies that the liquid must exhibit, at least, two anomalous properties in the supercritical region ($T > T_{C'}$): the increase of constant-pressure specific heat $[C_P(T, P)]$ and isothermal compressibility $[\kappa_T(T, P)]$ upon isobaric cooling. These anomalous properties are associated to the presence of minima and maxima in $\kappa_T(T, P)$ and $C_P(T, P)$ as function of temperature, at constant pressure. The location of these extrema in the $P-T$ plane define the minimum and maximum $\kappa_T(T, P)$ lines, $\kappa_{min}$ and $\kappa_{max}$ lines, respectively, as well as the minimum and maximum $C_P(T, P)$ lines, $C_P^{min}$ and $C_{P,max}$ line, respectively. In normal liquids, such lines do not exist; $\kappa_T(T, P)$ and $C_P(T, P)$ decrease monotonically upon isobaric cooling since these quantities are proportional to the liquids's volume and entropy fluctuations,[73] respectively, which usually become smaller as the system becomes more distant from the normal gas−liquid critical point. In the presence of the LLCP, $\kappa_T(T, P)$ and $C_P(T, P)$ decrease upon isobaric cooling at large enough $T$, as the liquid becomes more distant from the gas−liquid critical point, but at certain $T$ they must start to increase as the system approaches to the LLCP. For the temperatures below the LLCP, one can expect that $\kappa_T(T, P)$ and $C_P(T, P)$ must start to decrease upon cooling again.

In the case of water, computer simulations using the ST2, TIP4P/2005 and TIP5P models indicate that water has a single $\kappa_{max}$ line.[32,33,46] This $\kappa_{max}$ line originates at the LLCP and can be thought of an extension of the LLPT line (at $T < T_{C'}$) into the supercritical region.[71] Similarly, in the case of the Jagla model liquid, a $\kappa_{max}$ line originates at the LLCP and extends into the supercritical region with a positive slope. However, in this case, a second $\kappa_{max}$ line is observed (see Figure 5b of ref 52). This additional $\kappa_{max}$ line emerges from the minimum of the LDL spinodal line, where it crosses the maximum density line, and extends to higher temperatures in the $P$ vs $T$ plane with negative slope, until it crosses the maximum density line again at the point of its maximal temperature.

14233

dx.doi.org/10.1021/jp205098a |*J. Phys. Chem. B* 2011, 115, 14229−14239
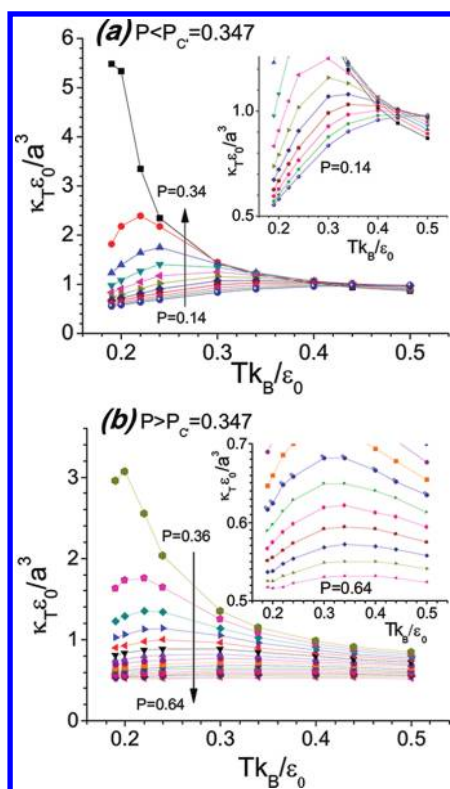
**Figure 5.** (a) Isothermal compressibility, $\kappa_T(T,P)$, as function of temperature at pressures (a) above and (b) below the LLCP pressure. Insets in (a) and (b) are a magnification of the corresponding panels at low temperature. The maxima of $\kappa_T(T,P)$ in (a) define the high-pressure $\kappa_{max}$ line of Figure 2a; the maxima in (b) define the low-pressure $\kappa_{max}$ line of Figure 2a.

Similarly to the Jagla model liquid, there are two $\kappa_{max}$ lines in the phase diagram of the Fermi–Jagla pair potential. Figures 2a and 2b show that one of the $\kappa_{max}$ lines is located above the LLCP, while the other exists below the LLCP. Simulations at high temperature show that the $\kappa_{max}$ lines merge into a common compressibility minimum line, $\kappa_{min}$ line, that expands from one $\kappa_{max}$ line to the other (not shown). The $\kappa_{max}$ line located at $P < P_{C'}$ corresponds to the maximum compressibility line that emerges from the LLCP. This line is analogous to the single $\kappa_{max}$ line observed in the computer simulations of water.[46] We note that the slope of this $\kappa_{max}$ line in the $P-T$ plane is negative since the slope of the LLPT line is also negative. Note that the $\kappa_{max}$ line located at $P > P_{C'}$ cannot be associated to the LLCP. This is because the $\kappa_{max}$ line that emerges from the LLCP should be a smooth extension of the LLPT line and thus, its slope should also be negative for $P \approx P_{C'}$. Instead, the slope of the $\kappa_{max}$ line located at $P > P_{C'}$ is positive for $P \approx P_{C'}$. The possibility for this $\kappa_{max}$ line to exhibit a change in slope at $P \approx P_{C'}$, and hence a minimum in the $P-T$ plane, should be ruled out. If this was the case, there should exist a $\kappa_{min}$ line in Figure 2b intersecting the $\kappa_{max}$ line at its minimum. A $\kappa_{min}$ line at $P \approx P_{C'}$ and $T > T_{C'}$ is not observed in the present simulations (Figure 2b).

In analogy with the Jagla model liquid (see Figure 5b of ref 52), one would expect that the $\kappa_{max}$ line located at $P > P_{C'}$ emerges from an extremum of the HDL spinodal line. It is difficult to discern from Figure 2b whether this is the case for the smooth pair potential. Moreover, since the HDL spinodal line in Figure 2b approaches the LLCP with approximately zero slope,

one could also expect that the $\kappa_{max}$ line (located at $P > P_{C'}$) emanates from the LLCP. Figure 2b suggest that this may be the case for the Fermi–Jagla potential. Elucidating the precise relationship among the $\kappa_{max}$ and spinodal lines requires a detailed characterization of the $P \approx P_{C'}$ region of the phase diagram; this issue will be addressed in a future work.

The plots of $\kappa_T(T,P)$ as function of temperature are shown in Figures 5a and 5b at $P < P_{C'}$ and $P > P_{C'}$, respectively. The maxima in these figures define the $\kappa_{max}$ lines of Figure 2. The maxima of $\kappa_T(P,T)$ increase as one moves along the $\kappa_{max}$ lines, approaching the LLCP.

As expected, we observe a $C_P^{min}$ line in the $(P, T)$ plane which goes almost vertically at $T \approx 0.75$ and expands approximately over the range $0 < P < 0.65$. One would also expect to observe a $C_P^{max}$ line emerging from the LLCP in Figure 2a. The $C_P^{max}$ line should collapse with the $\kappa_T^{max}$ line at temperatures $T \approx T_{C'}$ constituting the so-called 'Widom line'.[46] We run constant-pressure, cooling simulations in order to detect the $C_P^{max}$ line. However, no clear maxima were observed. We believe that this is because, in the present model liquid, the difference in entropy $(S)$ between LDL and HDL is small. This is because the slope of the LLPT line is small and, from the Clapeyron relationship, such a slope is proportional to $\Delta S = S_{HDL} - S_{LDL}$. Thus, since $C_P(T, P) = T(\partial S/\partial T)_P$, it follows that the change in $C_P(T, P)$, when going from LDL and HDL, should also be small resulting in weak specific heat maxima.

An interesting feature of Figure 2a is the presence of a density maximum line ($\rho_{max}$ line), defined as the set of temperatures at which the density reaches a maximum upon isobaric cooling. Its presence implies that the liquid exhibits a density anomaly, i.e., the existence of a range of temperatures at which the liquid expands upon isobaric cooling (normal liquids become denser upon cooling). As found in the case of water and Jagla model liquid,[52,70] the $\rho_{max}$ line in Figure 2a has a nose-like shape. For the Fermi–Jagla potential, the $\rho_{max}$ line extends up to a maximum temperature $T \approx 0.47$ (point "A" in the figure).

Sastry et al.[74] showed that an intimate relationship exists between the $\rho_{max}$ and $\kappa_T^{max}$ lines. Specifically, they showed that if the slope of the $\rho_{max}$ line in the $P-T$ plane is infinite [point A in Figure 2a] then the $\rho_{max}$ and $\kappa_{max}$ lines must intersect one another at that particular point. Figure 2a shows that this is indeed the case for the $\kappa_{max}$ line located at $P < P_{C'}$.

Thermodynamic arguments indicate that the $\rho_{max}$ line cannot end at finite temperature, in isolation. It must either terminate on a spinodal line[75] or merge with a minimum density line, $\rho_{min}$ line.[32] The $\rho_{min}$ line is defined as the set of temperatures in the $P-T$ plane at which the density of the liquid reaches a minimum upon isobaric cooling. For the Fermi–Jagla potential, it is found that, at low pressures, the $\rho_{max}$ and $\rho_{min}$ line merge with one another, see Figure 2a. However, at high pressures, there is no $\rho_{min}$ line and hence, the $\rho_{max}$ line must end at the LDL or HDL spinodal line.

To find out if the $\rho_{max}$ line terminates on the LDL or HDL spinodal line, and the precise point on such a spinodal line where the $\rho_{max}$ line indeed terminates, we consider the results of ref 75. In ref 75, it is shown that as the spinodal line is approached, it must be that

$$\frac{\alpha_P(T,P)}{dP_{spinodal}/dT} \rightarrow +\infty \text{ as } P \rightarrow P_{spinodal} \qquad (3)$$

were $\alpha_P(T,P)$ is the isobaric expansion coefficient, $dP_{spinodal}/dT$

14234

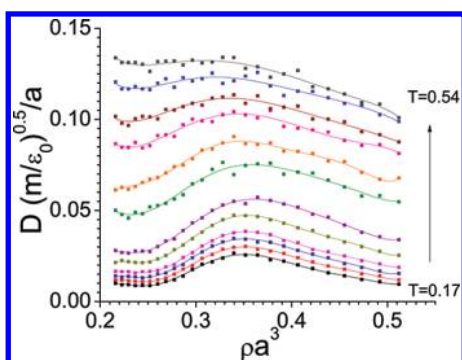dx.doi.org/10.1021/jp205098a |J. Phys. Chem. B 2011, 115, 14229–14239

**Figure 6.** Diffusion coefficient, $D(T,P)$, as function of density, $\rho = V/N$, for different temperatures. The maxima and minima of $D(T,P)$ define the $D_{max}$ and $D_{min}$ lines of Figure 2a, respectively. Lines are guide-to-the-eye obtained with 7-order polynomial interpolation.

is the slope of the spinodal line, and $P_{spinodal}$ is the pressure at the spinodal line, at the state point of interest. Figure 2b shows that $dP_{spinodal}/dT < 0$ along the LDL spinodal line, while $dP_{spinodal}/dT \geq 0$ along the HDL spinodal line. Since $\alpha_P(T,P) < 0$ on the left side of the $\rho_{max}$ line in Figure 2a, it follows that eq 3 can be satisfied only if the $\rho_{max}$ line terminates at the HDL spinodal line, crossing the LLPT coexistence line.[76] Moreover, since $\alpha_P(T,P) = 0$ along the $\rho_{max}$ line, it can be shown from eq 3 that, if the HDL spinodal line has a maximum, which could not be resolved with the available data in Figure 2a, then the $\rho_{max}$ line in Figure 2b must terminate at such a maximum; otherwise, the $\rho_{max}$ line must terminate at the LLCP, at which the HDL spinodal line in Figure 2b should have a zero slope. In both scenarios, given the shape of the HDL spinodal line in Figure 2b, the $\rho_{max}$ line would appear to emerge from the LLCP, as in Figure 2b.

**C. Dynamics.** Systems of particles interacting via core-softened pair potentials have the capability to exhibit diffusivity anomaly, i.e., the increase of diffusivity upon isobaric cooling. The Fermi−Jagla potential is not an exception. In fact, we find that the liquid exhibits a maximum diffusivity line ($D_{max}$ line), which is defined as the set of pressures at which the diffusion coefficient $D(T,P)$ is maximum upon isothermal compression. The $D_{max}$ line is shown in Figure 2a. Simulations also indicate the presence of a minimum diffusivity line [Figure 2a], $D_{min}$ line, at low pressures (the $D_{min}$ line is defined as the set of pressures at which $D(T,P)$ is minimal upon isothermal compression). In order to show that $D(T,P)$ has indeed maxima and minima at constant temperature, we show in Figure 6 the calculated $D(T,P)$ as function of density for different temperatures.

In the Jagla model liquid, HDL is a "strong" liquid,[5] the diffusion coefficient following an Arrhenius law

$$D = D_0 \exp\left(-\frac{E_A}{k_B T}\right) \qquad (4)$$

where the constant $E_A$ is the activation energy.[70] Instead, the LDL liquid is "fragile",[5] with the diffusion coefficient deviating from an Arrhenius law.[70] In the case of computer simulations of water[46] and silicon,[38] a similar situation regarding the diffusivity of the liquids holds. However, in these cases, the roles of LDL and HDL are exchanged: HDL is the fragile liquid, while LDL is the strong one. Whether LDL or HDL is the strong liquid is apparently correlated with the slope of the LLPT line and, hence, with the relative entropy of the liquids. In general, it is apparent
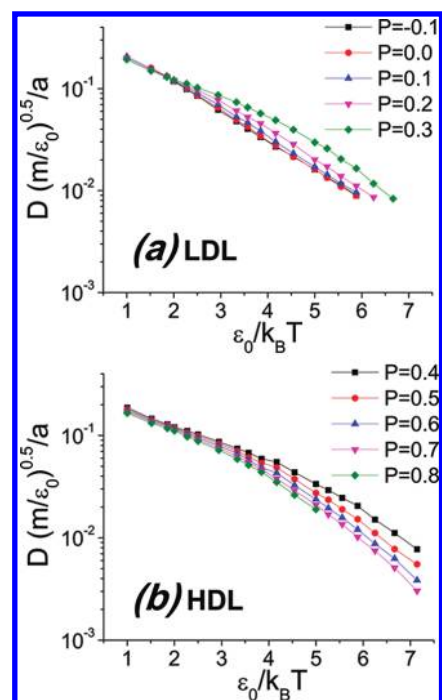


**Figure 7.** Arrhenius plot of the diffusion coefficient, $D(T,P)$, of (a) LDL and (b) HDL at different pressures. In the LDL case, $D(T,P)$ follows an Arrhenius law (eq 4). As the LLCP is approached ($P \to P_{C'} \approx 0.35$), deviation from the Arrhenius law occurs. In the HDL case, an Arrhenius law for $D(T,P)$ does not hold. Panels a and b suggest that LDL and HDL may be considered "fragile" and "strong" liquids, respectively, in Angell's classification of liquids dynamics.[5]

that the more ordered liquid is strong (it obeys eq 4), whereas the less ordered liquid is fragile.

For the smooth potential of eq 1, one would expect that LDL is strong and HDL is fragile, since the LLPT is negatively sloped in the $P$ vs $T$ plane, as found in water and silicon simulations. Figures 7a and 7b show $D(T,P)$ as function of temperature for LDL and HDL, respectively. Figure 7a shows that, as expected, LDL follows eq 4 at low pressures. As $P \to P_{C'}$, small deviations from the Arrhenius law can be observed. Instead, the data of Figure 7b for HDL cannot be fitted by eq 4, consistent with the view that HDL, being less ordered than LDL, is a fragile-like liquid.

## IV. GLASS POLYMORPHISM: LOW-DENSITY AND HIGH-DENSITY AMORPHOUS SOLIDS

Most polymorphic liquids also show, or are believed to show, polyamorphism in the glass state. Examples include water,[72] silicon,[77,78] and $Al_2O_3-Y_2O_3$ melts.[18,56] Other systems, such as tetrahedral[26,27] and core-softened pair interaction liquids,[16,52] may also exhibit liquid and/or glass polymorphism. In this section, we study the glass behavior of the Fermi−Jagla pair potential. Specifically, we explore (i) whether this model liquid is able to exhibit the pressure-induced amorphization (PIA) of its low pressure crystal, and (ii) whether it exhibits glass polymorphism. This is particular relevant for the Fermi−Jagla pair potential given the rapid crystallization that usually occurs in MD simulations of systems of particles with smooth interactions.

**A. High- and Low-Density Amorphous Solids.** Experiments in water show that isothermal compression of hexagonal ice
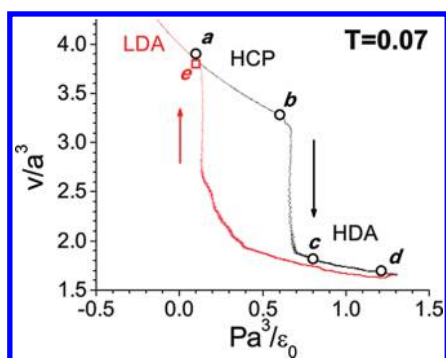
**Figure 8.** Volume per particle as function of pressure upon compression of the low pressure (HCP) crystal at $T = 0.07$ (black line) and subsequent decompression at the same temperature (red line). The HCP crystal transforms to HDA at $P = 0.68$ via an apparent first-order phase transition. Decompression of HDA results in LDA at $P \approx 0.14$. The radial distribution function of the system at state points $a$, $b$, $c$, $d$, and $e$ are shown in Figure 9.



**Figure 9.** Radial distribution functions (RDFs) during the compression-induced HCP-to-HDA transformation and subsequent decompression-induced HDA-to-LDA transformation at $T = 0.07$. The RDFs correspond to state points marked by $a$ (HCP, $P = 0.10$), $b$ (HCP, $P = 0.60$), $c$ (HDA, $P = 0.80$), $d$ (HDA, $P = 1.21$), and $e$ (LDA, $P = 0.10$) in Figure 8. The RDF corresponding to state point $a$ (HCP, $P = 0.10$) is shown in both panels a and c.

(the low-pressure, equilibrium form of ice) at $T = 77$ K produces HDA at $P > 1$ GPa.[1] Similarly, MD simulations using the Jagla model show that isothermal compression of the corresponding low-pressure crystal results in an HDA solid.[51] Next, we test whether PIA of the low-pressure crystal of our smooth pair potential, hexagonal closed packed (HCP) crystal, also produces HDA.

In order to form HDA, we first take an HCP crystal configuration at $T = 0.16$ and $P = -0.19$ formed spontaneously upon cooling the liquid at constant $V = 19.8^3 = 7762.4$ at our standard cooling rate $q_T = 10^{-4}$. The system is then compressed at constant temperature up to $P = 0.1$ and then cooled isobarically to the desired compression temperature. After thermalizing the system for $10^5$ time steps, the HCP crystal configuration is compressed. HCP crystal is compressed at $T = 0.01, 0.03, 0.05, 0.07$, and $0.10$, below the crystallization line of LDL [Figure 2a]. In all cases, HCP crystal transforms to HDA rather suddenly. For example, the volume of the system as function of pressure upon compression HCP crystal at $T = 0.07$ is shown in Figure 8. The sudden change in volume at $P = 0.68$ indicates that the HCP-to-HDA transformation is an apparent first-order phase transition. The compression curve of Figure 8 is remarkably similar to the compression curve obtained in the PIA of ice $I_h$ in ref 1.

The structure of HCP crystal and HDA at $T = 0.07$ are shown in Figure 9, panels a and b, respectively. Figure 9a shows that, as expected, the RDF of HCP crystal exhibits long-range order as indicated by the maxima and minima at large values of $r$. Compression of HCP crystal up to $P = 0.60$, before the HCP-to-HDA transformation occurs, results in an elastic deformation (i.e., $P$ is practically a linear function of $v$; Figure 8). In this range of pressures, particles get closer to one another and the peaks of the RDF shift to lower values of $r$. Comparison of the RDFs of HCP crystal at $P = 0.10$ and $P = 0.60$ indicates that the main features of the RDF remain, although the RDF starts to become smoother as the transformation pressure is approached (see, e.g., the first double peak of the RDF at $r \approx 2.2-3.8$). During the transformation from HCP crystal to HDA, particles move from separations $r_1 \approx 1.7$ (first peak of the RDF of HCP crystal) to separations $r_2 \approx 1$. The same particle rearrangement was observed in the LDL-to-HDL transformation (section III.A). We note that HDA is indeed amorphous, as evidenced by the lack
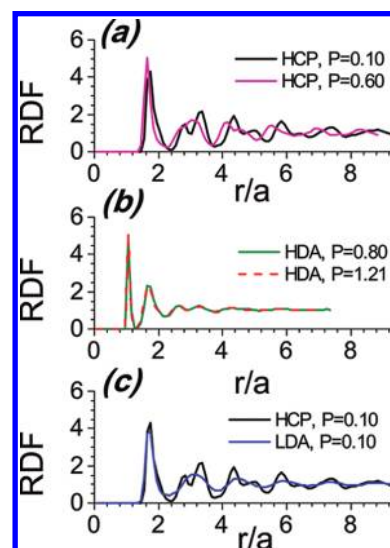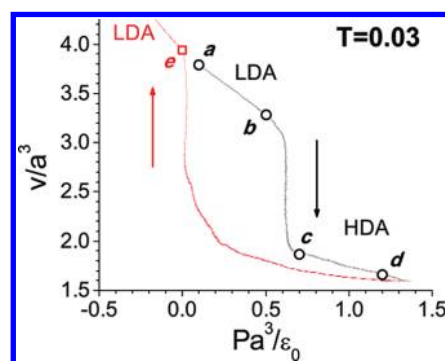


**Figure 10.** Volume per particle as function of pressure upon compression of LDA at $T = 0.03$ (black line) and subsequent decompression at the same temperature (red line). LDA transforms to HDA at $P = 0.62$ via an apparent first-order phase transition. Decompression of HDA results in LDA at $P \approx 0.01$. The radial distribution function of the system at points $a$, $b$, $c$, $d$, and $e$ are shown in Figure 11.

of long-range order in its RDF [Figure 9b]. Specifically, the RDF of HDA is almost flat for $r > 4.2$.

Included in Figure 8 is the $v(P)$ curve upon decompression of HDA at $T = 0.07$. Figure 8 may be misleading since it could be interpreted as indicating that the HCP-to-HDA transformation is apparently reversible, in the sense that the system can be brought back to the starting pressure and temperature. In fact, the HCP-to-HDA transformation is not reversible. A close look to the system's structure after decompression at $P = 0.1$ reveals that the system is indeed amorphous; that is, decompression of HDA produces an LDA solid. The RDF of LDA is shown in Figure 9c. The RDFs of LDA and HCP crystal resemble one another. However, LDA has only short-range order since its RDF is mainly flat for approximately $r > 6$.
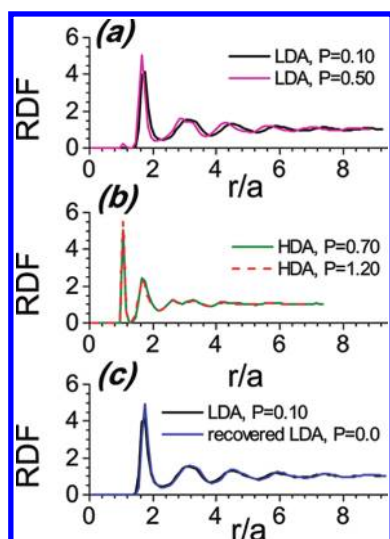
**Figure 11.** Radial distribution functions (RDFs) during the compression-induced LDA-to-HDA transformation and subsequent decompression-induced HDA-to-LDA transformation at $T = 0.03$. The RDFs correspond to state points marked by $a$ (LDA, $P = 0.10$), $b$ (LDA, $P = 0.50$), $c$ (HDA, $P = 0.70$), $d$ (HDA, $P = 1.20$), and $e$ (recovered LDA, $P = 0.0$) in Figure 10. The RDF corresponding to state point $a$ (LDA, $P = 0.10$) is shown in both panels a and c.

**B. Apparent First-Order Phase Transition between Low- and High-Density Amorphous Solids.** In polymorphic glasses, LDA and HDA can usually be interconverted by isothermal compression and/or decompression. This is the case of, e.g., water[79,80] and $Ce_{55}Al_{45}$,[16] and the common situation observed in computer simulations.[10,38,51,81] To test whether this scenario also holds for the Fermi—Jagla potential, we compress LDA at $T = 0.01, 0.03, 0.05, 0.07$, and $0.10$ at the same compression rate used in section IV.A for the compression of HCP crystal. LDA is prepared by cooling the liquid isobarically at $P = 0.01$ to the desired compression temperature. We use a fast cooling rate of $q_T = 10^{-3}$ in order to avoid crystallization.

We observed that crystallization occurs during the compression of LDA at $T = 0.05, 0.07$, and $0.10$. The crystal forms before LDA can transform to HDA. Crystallization cannot be avoided at these temperatures even if the compression rate is increased by a factor of 10. At $T = 0.01$ and $0.03$, crystallization can be avoided and the LDA-to-HDA transformation is observed. The pressure-dependence of the system's volume upon compressing LDA at $T = 0.03$ is shown in Figure 10. The LDA-to-HDA transformation occurs at $P = 0.62$, as indicated by the sharp change in volume observed in Figure 10. During the LDA-to-HDA transformation $(\partial P / \partial V)_T \approx 0$ and thus, the transformation resembles a first-order phase transition. Upon decompression of HDA at $T = 0.03$, LDA suddenly forms at $P = 0.01$ via an apparent first-order phase transition (Figure 10). Thus, similar to the case of water,[72] the LDA-to-HDA transformation is reversible in the present model liquid.

The structures of the different glasses are compared in Figure 11. Figure 11a shows the RDF of LDA at $P = 0.1$ and $P = 0.5$, just before it transforms to HDA. The similarities in these RDFs clearly indicate that only minor structural changes occur at $P \leq 0.5$. Comparison of the RDFs of LDA at $P = 0.5$ and $T = 0.03$, Figure 11a, and HCP crystal at $P = 0.6$ and $T = 0.07$, Figure 9a, shows minor differences in the structure of HCP and LDA

just before they transform to HDA. However, the RDF of HCP crystal shows sharper maxima and minima than those observed in the RDF of LDA, even when the HCP crystal is at a higher temperature than LDA.

The RDFs of HDA in Figures 11b and 9b practically overlap indicating that the same HDA form is obtained upon compression of HCP crystal and LDA. Accordingly, the RDFs of recovered LDA in Figures 11c and 9c also overlap. That the LDA-to-HDA transformation is indeed reversible is supported by Figure 11c. Specifically, this figure shows that the RDFs of the starting LDA at $P = 0.1$ and recovered LDA at the same pressure practically overlap; that is, they have the same amorphous structure.

## V. SUMMARY AND DISCUSSION

In this work, we have introduced a smooth pair interaction potential based on the Jagla pair potential that was originally used to study the anomalous properties of water and silica. We call this new potential the Fermi—Jagla potential, because we replace the linear ramps of the original Jagla potential by Fermi functions. While the Jagla pair potential leads to forces between particles that are discontinuous functions of the interparticle separations, this is not the case of the Fermi—Jagla potential. Therefore, contrary to the Jagla model case, systems of particles interacting via the Fermi—Jagla potential can be simulated using standard MD techniques. What makes the Fermi—Jagla potential interesting, in comparison to other common smooth potentials, is that it exhibits liquid and glass polymorphism, as in the original Jagla model. We note that even though the Fermi—Jagla and Jagla pair potentials have similar form, it is not obvious that they should shear similar thermodynamic properties since minor details in pair interaction potentials can lead to drastically different thermodynamic, structural, and/or dynamical properties.

The main difference between the Jagla and Fermi—Jagla potentials is the slope of the corresponding LLPT line. Such a slope is positive in the Jagla liquid while it is slightly negative in the Fermi—Jagla potential liquid case. Experiments indicate that most of the known polyamorphic substances, such as water, silicon, and yttrium oxide—aluminum oxide melts have, or are expected to have, LLPT with negative slopes in the $P$ vs $T$ plane. In this regard, the Fermi—Jagla potential is a step forward toward the modeling of the thermodynamic properties of these substances. The fact that the LLPT is well separated from the crystallization region in the smooth potential liquid, suggests that reparametrization of the model may lead to liquids with LLPT lines that have larger negative slopes than in the present case study, as well as positive slopes. We are currently studying the effects of different parametrization of the smooth pair potential on the LLPT line and will present the results in a separate work.

We have presented a detailed characterization of the anomalous properties of the liquid in the supercritical region. Specifically, we were able to locate maximum and minimum (i) density, (ii) compressibility, and (iii) diffusivity lines. We also found a minima line of constant-pressure specific heat. However, we could not identify a maxima line associated to the constant-pressure specific heat. Although such a maxima line must emerge from the LLCP, the similar entropies of LDL and HDL (indicated by the small slope of the LLPT line) may make it difficult to detect maxima in $C_P(T,P)$.

Regarding the dynamical properties of the liquids, we showed that LDL, the more ordered liquid, is strong while HDL, the less

ordered liquid, is fragile. These results are consistent with previous work on polymorphic liquids indicating that the strong versus fragile behavior of the LDL and HDL phases is associated with their entropies rather than densities, so that the more ordered phase is strong, while the less ordered phase is fragile. Accordingly, the dynamic properties of LDL and HDL are consistent with the observation that the LLPT line is negatively sloped in the Fermi−Jagla model liquid.

In the last section of this work we showed that the Fermi−Jagla model system exhibits glass polymorphism. Specifically, it was shown that the model exhibits the (i) crystal-to-HDA and (ii) reversible LDA−HDA transformations that are commonly observed in experiments of polyamorphic substances. A detailed characterization of the crystallization and glass phenomenology of the Fermi−Jagla model system will be presented in a separate work. The fact that polyamorphism can be studied in the present model system makes it a remarkable tool for the study of the phenomenology of glasses, glass polymorphism, and the glass transition using MD simulations (in general, smooth pair interaction potential easily crystallize, even in short MD simulation time scales).

## ■ REFERENCES

(1) Mishima, O.; Calvert, L. D.; Whalley, E. *Nature* **1984**, *310*, 393.
(2) Mishima, O.; Calvert, L. D.; Whalley, E. *Nature* **1985**, *314*, 76.
(3) McMillan, P. F.; Wilson, M.; Wilding, M. C.; Daisenberger, D.; Mezouar, M.; Greaves, G. N. *J. Phys.: Condens. Matter* **2007**, *19*, 415101.
(4) McMillan, P. F. *J. Mater. Chem.* **2004**, *14*, 1506.
(5) Angell, C. A. *Science* **1995**, *267*, 1924.
(6) Mishima, O.; Stanley, H. E. *Nature* **1998**, *396*, 329.
(7) Tanaka, H. *Phys. Rev. E* **2000**, *62*, 6968.
(8) Rapoport, E. *J. Chem. Phys.* **1967**, *46*, 2891.
(9) Ponyatovsky, E. G. *J. Phys.: Condens. Matter* **2003**, *15*, 6123.
(10) Poole, P. H.; Sciortino, F.; Essmann, U.; Stanley, H. E. *Nature* **1992**, *360*, 324.
(11) Beye, M.; Sorgenfrei, F.; Schlotter, W. F.; Wurth, W.; Föhlisch, A. *Proc. Natl. Acad. Sci. U.S.A.* **2010**, *107*, 16772.
(12) Bhat, M. H.; Molinero, V.; Soignard, E.; Solomon, V. C.; Sastry, S.; Yarger, J. L.; Angell, C. A. *Nature* **2007**, *448*, 787.
(13) Katayama, Y.; Mizutani, T.; Utsumi, W.; Shimomura, O.; Yamakata, M.; Funakosh, K. *Nature* **2000**, *403*, 170.
(14) Monaco, G.; Falconi, S.; Crichton, W. A.; Mezouar, M. *Phys. Rev. Lett.* **2003**, *90*, 255701.
(15) Grimsditch, M. *Phys. Rev. Lett.* **1984**, *52*, 2379.
(16) Sheng, H. W.; Liu, H. Z.; Cheng, Y. Q.; Wen, J.; Lee, P. L.; Luo, W. K.; Shastry, S. D.; Ma, E. *Nat. Mater.* **2007**, *6*, 192.
(17) Zeng, Q.-S.; Ding, Y.; Mao, W. L.; Yang, W.; Sinogeikin, S. V.; Shu, J.; Mao, H.-K.; Jiang, J. Z. *Phys. Rev. Lett.* **2010**, *104*, 105702.
(18) Aasland, S.; McMillan, P. F. *Nature* **1994**, *369*, 633.
(19) Kurita, R.; Tanaka, H. *J. Phys.: Condens. Matter* **2005**, *17*, L293.
(20) Bolshakov, B. V.; Dzhonson, A. G. *Dokl. Phys. Chem.* **2003**, *393*, 318.
(21) Tanaka, H.; Kurita, R.; Mataki, H. *Phys. Rev. Lett.* **2004**, *92*, 025701.
(22) Kurita, R.; Tanaka, H. *Science* **2004**, *306*, 845.
(23) Cohen, I.; Ha, A.; Zhao, X.; Lee, M.; Fischer, T.; Strouse, M. J.; Kivelson, D. *J. Phys. Chem.* **1996**, *100*, 8518.

(24) Kurita, R.; Murata, K.-I.; Tanaka, H. *Nat. Mater.* **2008**, *7*, 647.
(25) Brazhkin, V. V.; Lyapin, A. G. *J. Phys.: Condens. Matter* **2003**, *15*, 6059.
(26) Angell, C. A.; Bressel, R. D.; Hemmatti, M.; Sare, E. J.; Tucker, J. C. *Phys. Chem. Chem. Phys.* **2000**, *2*, 1559.
(27) Poole, P. H.; Grande, T.; Angell, C. A.; McMillan, P. F. *Science* **1997**, *275*, 322.
(28) Kiss, Z. J.; Pressley, R. J. *Appl. Opt.* **1966**, *5*, 1474.
(29) Levy, Y.; Onuchic, J. N. *Annu. Rev. Biophys. Biomol. Struct.* **2006**, *35*, 389.
(30) Ball, P. *Chem. Rev.* **2008**, *108*, 74.
(31) Loerting, L.; Giovambattista, N. *J. Phys.: Condens. Matter* **2006**, *18*, R919.
(32) Poole, P. H.; Saika-Voivod, I.; Sciortino, F. *J. Phys.: Condens. Matter* **2005**, *17*, L431.
(33) Abascal, J. L. F.; Vega, C. *J. Chem. Phys.* **2010**, *133*, 234502.
(34) Jedlovszky, P.; Vallauri, R. *J. Chem. Phys.* **2005**, *122*, 081101.
(35) Yamada, M.; Mossa, S.; Stanley, H. E.; Sciortino, F. *Phys. Rev. Lett.* **2002**, *88*, 195701.
(36) Saika-Voivod, I.; Poole, P. H.; Sciortino, F. *Nature* **2001**, *412*, 514.
(37) Stillinger, F. H.; Weber, T. A. *Phys. Rev. B* **1985**, *31*, 5262.
(38) Sastry, S.; Angell, C. A. *Nature Mat.* **2003**, *2*, 739.
(39) Vasisht, V. V.; Saw, S.; Sastry, S. *Nat. Mater.* **2011**.
(40) Molinero, V.; Sastry, S.; Angell, C. A. *Phys. Rev. Lett.* **2006**, *97*, 075701.
(41) Hemmer, P. C.; Stell, G. *Phys. Rev. Lett.* **1970**, *24*, 1284.
(42) Stell, G.; Hemmer, P. C. *J. Chem. Phys.* **1972**, *56*, 4274.
(43) Stillinger, F. H.; Stillinger, D. K. *Physica A* **1997**, *244*, 358.
(44) Yan, Z.; Buldyrev, S. V.; Kumar, P.; Giovambattista, N.; Stanley, H. E. *Phys. Rev. E* **2008**, *77*, 042201.
(45) Jagla, E. A. *Phys. Rev. E* **2001**, *63*, 061509.
(46) Xu, L.; Kumar, P.; Buldyrev, S. V.; Chen, S.-H.; Poole, P. H.; Sciortino, F.; Stanley, H. E. *Proc. Natl. Acad. Sci. U.S.A.* **2005**, *102*, 16558.
(47) Jagla, E. A. *J. Chem. Phys.* **1999**, *111*, 8980.
(48) Jagla, E. A. *Phys. Rev. E* **2001**, *63*, 061501.
(49) Franzese, G. *J. Mol. Liq.* **2007**, *136*, 267.
(50) Xu, L.; Buldyrev, S. V.; Giovambattista, N.; Angell, C. A.; Stanley, H. E. *J. Chem. Phys.* **2009**, *130*, 054505.
(51) Xu, L.; Giovambattista, N.; Buldyrev, S. V.; Debenedetti, P. G.; Stanley, H. E. *J. Chem. Phys.* **2011**, *134*, 064507.
(52) Buldyrev, S. V.; Malescio, G.; Angell, C. A.; Giovambattista, N.; Prestipino, S.; Saija, F.; Stanley, H. E.; Xu, L. *J. Phys.: Condens. Matter* **2009**, *21*, 504106.
(53) Buldyrev, S. V.; Franzese, G.; Giovambattista, N.; Malescio, G.; Sadr-Lahijany, M. R.; Scala, A.; Skibinsky, A.; Stanley, H. E. *Physica A* **2003**, *304*, 23.
(54) Gibson, H. M.; Wilding, N. B. *Phys. Rev. E* **2006**, *73*, 061507.
(55) Daisenberger, D.; Wilson, M.; McMillan, P. F.; Quesada Cabrera, R.; Wilding, M. C.; Machon, D. *Phys. Rev. B* **2007**, *75*, 224118.
(56) Greaves, G. N.; Wilding, M. C.; Fearn, S.; Langstaff, D.; Kargl, F.; Cox, S.; Vu Van, Q.; Majé rus, O.; Benmore, C. J.; Weber, R.; Martin, C. M.; Hennet, L. *Science* **2008**, *322*, 566.
(57) Barros de Oliveira, A.; Franzese, G.; Netz, P. A.; Barbosa, M. C. *J. Chem. Phys.* **2008**, *128*, 064901.
(58) Vilaseca, P.; Franzese, G. *J. Chem. Phys.* **2010**, *133*, 084507.
(59) Barros de Oliveira, A.; Netz, P. A.; Colla, T.; Barbosa, M. C. *J. Chem. Phys.* **2006**, *124*, 084505.
(60) Barros de Oliveira, A.; Netz, P. A.; Colla, T.; Barbosa, M. C. *J. Chem. Phys.* **2006**, *125*, 124503.
(61) Gribova, N. V.; Fomin, Y. D.; Frenkel, D.; Ryzhov, V. N. *Phys. Rev. E* **2009**, *79*, 051202.
(62) Krekelberg, W. P.; Kumar, T.; Mittal, J.; Errington, J. R.; Truskett, T. M. *Phys. Rev. E* **2009**, *79*, 031203.
(63) Barros de Oliveira, A.; Netz, P. A.; Barbosa, M. C. *EPL* **2009**, *85*, 36001.
(64) Camp, P. J. *Phys. Rev. E* **2003**, *68*, 061506.

14238

dx.doi.org/10.1021/jp205098a |*J. Phys. Chem. B* 2011, 115, 14229–14239

(65) Camp, P J. *Phys. Rev. E* **2005**, *71*, 031507.

(66) Yan, Z.; Buldyrev, S. V.; Giovambattista, N.; Stanley, H. E. *Phys. Rev. Lett.* **2005**, *95*, 130604.

(67) Yan, Z.; Buldyrev, S. V.; Giovambattista, N.; Debenedetti, P. G.; Stanley, H. E. *Phys. Rev. E* **2006**, *73*, 051204.

(68) Rapaport, D. C. *The Art of Molecular Dynamics Simulations*; Cambridge University Press: New York, 1995.

(69) Berendsen, H. J. C.; Postma, J. P. M.; van Gunsteren, W. F.; DiNola, A.; Haak, J. R. *J. Phys. Chem.* **1984**, *81*, 3684.

(70) Xu, L.; Buldyrev, S. V.; Angell, C. A.; Stanley, H. E. *Phys. Rev. E* **2006**, *74*, 031108.

(71) Callen, H. B. *Thermodynamics and an Introduction to Thermostatistics*; John Willey Sons: New York, 1985.

(72) Mishima, O. *J. Phys. Chem.* **1994**, *100*, 5910.

(73) Debenedetti, P. G.; Stanley, H. E. *Phys. Today* **2003**, *56*, 40.

(74) Sastry, S.; Debenedetti, P. G.; Sciortino, F.; Stanley, H. E. *Phys. Rev. E* **1996**, *53*, 6144.

(75) Speedy, R. J. *J. Phys. Chem.* **1982**, *86*, 982.

(76) We note that in our simulations, the $\rho_{max}$ line cannot terminate at the LL coexistence line. This is because the liquid at high pressures and at $T < T_{C'}$ remains in the HDL phase until the HDL-to-LDL spinodal pressure is reached. Thus, HDL is unaware of the presence of any LL coexistence line. Since the $\rho_{max}$ line at $P > P_{C'}$ and $T < T_{C'}$ occurs in the HDL phase, this line extends until the HDL-to-LDL spinodal line is reached, at which HDL transforms to LDL in the simulation. An analogous situation was observed in the case of the Jagla model liquid where the slope of the LL coexistence line is more pronounced and positive. In this case, the $\rho_{max}$ line at $T < T_{C'}$ occurs in the LDL phase and it extends until it intersects the minimum of the LDL-to-HDL spinodal line.

(77) Deb, S. K.; Wilding, M.; Somayazulu, M.; McMillan, P. F. *Nature* **2001**, *414*, 538.

(78) McMillan, P. F.; Wilson, M.; Daisenberger, D.; Machon, D. *Nat. Mater.* **2005**, *4*, 680.

(79) Winkel, K; Bauer, M.; Mayer, E.; Seidl, M.; Elsaesser, M. S.; Loerting, T. *J. Phys.: Cond. Matter* **2008**, *20*, 494212.

(80) Loerting, T.; Schustereder, W.; Winkel, K.; Salzmann, C. G.; Kohl, I.; Mayer, E. *Phys. Rev. Lett.* **2006**, *96*, 025702.

(81) Giovambattista, N.; Stanley, H. E.; Sciortino, F. *Phys. Rev. E* **2005**, *72*, 031510.